

Energy-pooling collisions in cesium: $6P_J + 6P_J \rightarrow 6S + (nl = 7P, 6D, 8S, 4F)$

Z. J. Jabbour,* R. K. Namiotka, and J. Huennekens

Department of Physics, Lehigh University, 16 Memorial Drive East, Bethlehem, Pennsylvania 18015

M. Allegrini,† S. Milošević,‡ and F. de Tomasi§

Unità INFN, Dipartimento di Fisica, Università di Pisa, Piazza Torricelli 2, 56126 Pisa, Italy

(Received 25 September 1995)

We report experimental rate coefficients for the energy-pooling collisions $\text{Cs}(6P_{1/2}) + \text{Cs}(6P_{1/2}) \rightarrow \text{Cs}(6S_{1/2}) + \text{Cs}(nl_{J'})$ and $\text{Cs}(6P_{3/2}) + \text{Cs}(6P_{3/2}) \rightarrow \text{Cs}(6S_{1/2}) + \text{Cs}(nl_{J'})$ where $nl_{J'} = 7P_{1/2}, 7P_{3/2}, 6D_{3/2}, 6D_{5/2}, 8S_{1/2}, 4F_{5/2},$ or $4F_{7/2}$. Atoms were excited to either the $6P_{1/2}$ or $6P_{3/2}$ state using a single-mode Ti:sapphire laser. The excited-atom density and spatial distribution were mapped by monitoring the absorption of a counterpropagating single-mode ring dye laser beam, tuned to either the $6P_{1/2} \rightarrow 8S_{1/2}$ or $6P_{3/2} \rightarrow 7D_{3/2,5/2}$ transitions, which could be translated parallel to the pump beam. Transmission factors, which describe the average probability that photons emitted within the fluorescence detection region can pass through the optically thick vapor without being absorbed, were calculated for all relevant transitions. Effective lifetimes of levels populated by energy-pooling collisions are modified by radiation trapping, and these factors were calculated using the Molisch theory. These calculated quantities have been combined with the measured excited-atom densities and fluorescence ratios to yield absolute energy-pooling rate coefficients. It was found that the rate for production, in all cases, is greatest for $6D$, but that $1/2-1/2$ collisions are significantly more efficient than $3/2-3/2$ collisions for populating $7P$. It was also found that $7P_{1/2}$ is populated two to three times more efficiently than $7P_{3/2}$ in $1/2-1/2$ collisions, but that the $7P$ fine-structure levels are approximately equally populated in $3/2-3/2$ collisions. [S1050-2947(96)00508-2]

PACS number(s): 34.50.Rk, 34.90.+q

I. INTRODUCTION

In 1972, Klyucharev and Lazarenko [1] reported that when cesium vapor was resonantly excited to the $6P$ levels, fluorescence from the $6D$ atomic levels, which lie near twice the $6P$ energy, could be observed. The population in the high-lying levels was attributed to excited-atom-excited-atom collisions in which the two atoms pool their internal energy to produce one ground-state atom and one in a more highly excited state $nl_{J'}$ (in this case $nl_{J'} = 6D_{3/2,5/2}$)

$$\text{Cs}(6P_J) + \text{Cs}(6P_J) \Rightarrow \text{Cs}(nl_{J'}) + \text{Cs}(6S_{1/2}). \quad (1)$$

Collisions of this type have since come to be called “energy-pooling collisions” and they have been the subject of much study in alkali-metal homonuclear [2–5] and heteronuclear [6,7] systems, as well as in other metal vapors [8–15] over the last 20 years.

While the majority of previous alkali-metal work has concentrated on sodium, [2–4] there has been little work on cesium following the initial paper by Klyucharev and Laza-

renko. However, energy pooling in cesium is of current interest because such collisions could be an important loss mechanism in ultracold laser traps, especially now that trap densities of 10^{11} to 10^{12} cm^{-3} are within range [16]. In addition, the large fine-structure of the cesium $6P_J$ levels makes the study of cesium energy pooling more interesting, since the combinations $6P_{1/2} + 6P_{1/2}$, $6P_{1/2} + 6P_{3/2}$, and $6P_{3/2} + 6P_{3/2}$ are more or less resonant with various highly excited states (see Fig. 1). The large fine-structure splittings also allow study of the role of angular momentum in the energy-pooling process. To the best of our knowledge, there have been only a few quantitative studies to date on energy pooling in cesium. In their original paper, Klyucharev and Lazarenko [1] estimated from experiment that the cross section for process (1) was less than 10^{-13} cm^2 for $nl = 6D$ at a temperature of 528 K. Later, Borodin and Komarov [17] determined theoretically that the cross section exceeds 1.5×10^{-15} cm^2 for this process at $T = 500$ K. Yabuzaki *et al.* [18] carried out an experimental study of the inverse process, $\text{Cs}(6D) + \text{Cs}(6S) \rightarrow \text{Cs}(6P) + \text{Cs}(6P)$ and found a cross section of $(1.5_{-0.7}^{+1.5}) \times 10^{-14}$ cm^2 at 530 K. Preliminary experimental results on the process $\text{Cs}(6P_{3/2}) + \text{Cs}(6P_{3/2}) \rightarrow \text{Cs}(7P_{J'}) + \text{Cs}(6S_{1/2})$ have recently been obtained [19] and additional results for $6P_{1/2}$ excitation, along with details of the $6P_{3/2}$ experiment will appear shortly [20].

It is the purpose of this manuscript to present quantitative experimental results for rate coefficients and cross sections for the cesium energy-pooling process [Eq. (1)]. Such measurements are complicated by the need to know both the density and the spatial distribution of excited atoms in the vapor. In this work, the excited-atom density and spatial distribution were measured using a weak probe laser. In addi-

*Present address: Automated Production Technology Division, Sound A147, NIST, Gaithersburg, Maryland 20899.

†Present address: Dipartimento di Fisica della Materia, Geofisica e Fisica dell’Ambiente, Università di Messina, Salita Sperone 31, 98166 Sant’ Agata, Messina, Italy.

‡Permanent address: Institute of Physics, University of Zagreb, P.O. Box 304, Zagreb 41000, Croatia.

§Present address: Laboratoire de Physique des Lasers, Université Paris-Nord, Avenue J. B. Clement, 93430 Villetaneuse, France.

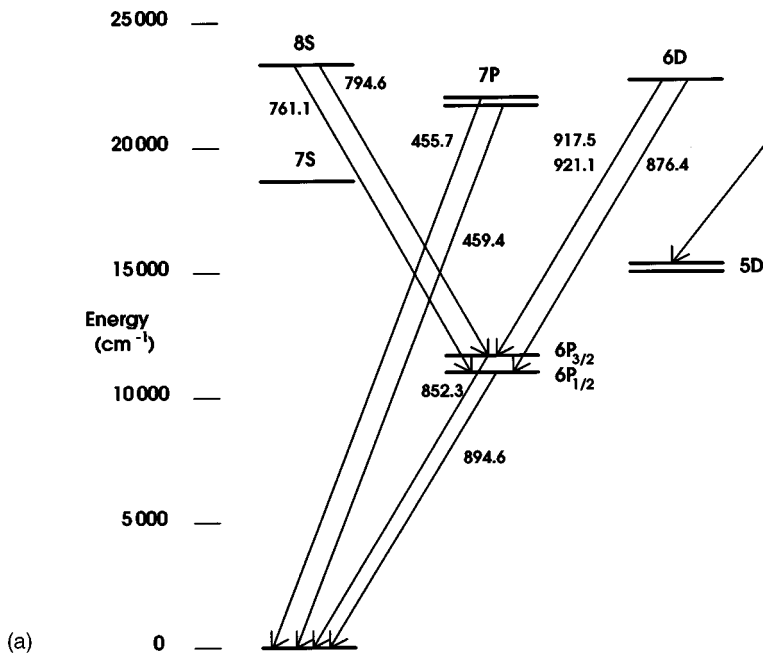
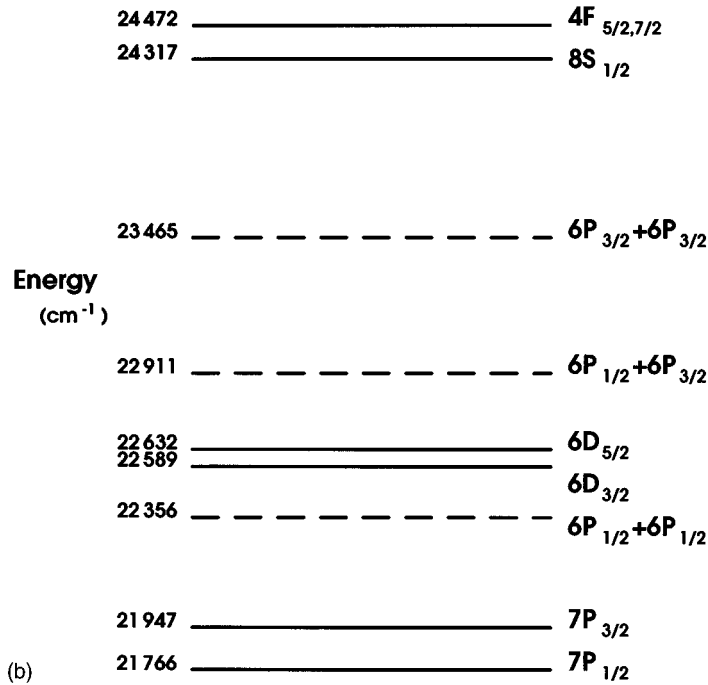


FIG. 1. (a) Energy levels of cesium showing transitions studied in this work. Wavelengths are given in nm. (b) Cesium atomic levels lying near twice the $6P_J$ level energies. $6P_J + 6P_J$ energies are represented by dashed lines. Energies are taken from Ref. [56].



tion, radiation trapping, radiative cascade, optical pumping, and other effects must also be considered. Rate coefficients for energy pooling with product states $nl_J' = 7P_{1/2}$, $7P_{3/2}$, $6D_{3/2}$, $6D_{5/2}$, $8S_{1/2}$, $4F_{5/2}$, and $4F_{7/2}$ are reported.

This paper is organized as follows. Section II presents a rate equation model used to extract the energy-pooling rate coefficients from the measured fluorescence ratios. It also discusses radiation trapping and related optical depth problems in detail. Experimental details, including a description of the excited-atom density measurement are presented in Sec. III. Results are given in Sec. IV along with a discussion of various sources of error. Finally, our conclusions are presented in Sec. V.

II. THEORY

A. Rate equations

The energy-pooling process described by Eq. (1) produces atoms in the highly excited states nl_J' which lie near twice the energy of the pumped resonance state [see Fig. 1(b)]. Rate equations can be used to derive theoretical expressions for the populations in these higher excited states, which in turn yield expressions for the energy-pooling rate coefficients. Note that, for the most part, this discussion follows that of Neuman, Gallagher, and Cooper [15]. The steady-state rate equation for the population in state nl_J' following pumping of $6P_J$ reads

$$\dot{n}_{nl_j}(\vec{r})=0=\frac{k_{nl_j}[n_{6P_j}(\vec{r})]^2}{2}-\frac{n_{nl_j}(\vec{r})}{\tau_{nl_j}^{\text{eff}}}, \quad (2)$$

which has the solution

$$n_{nl_j}(\vec{r})=\frac{1}{2}k_{nl_j}[n_{6P_j}(\vec{r})]^2\tau_{nl_j}^{\text{eff}}, \quad (3)$$

Here, k_{nl_j} is the rate coefficient for process (1), and $\tau_{nl_j}^{\text{eff}}$ is the effective lifetime for atoms in state nl_j . Note that in the absence of quenching collisions and radiation trapping, $(\tau_{nl_j}^{\text{eff}})^{-1}$ is just the sum of the Einstein A coefficients for transitions connecting state nl_j to all lower levels. However, at higher atom densities, radiation trapping will reduce the effective radiative rate for transitions to the ground state. We will find that radiation trapping can also occur, under some circumstances, for transitions terminating on levels directly populated by the laser. Note that the factor 2 introduced in Eq. (2) is due to the fact that the $6P_j$ atoms are identical. Therefore $[n_{6P_j}]^2/2$ is proportional to the number of excited-atom pairs in the volume, as first pointed out in Ref. [21].

We are interested in the fluorescence corresponding to the transition $nl_j \rightarrow n'l'_j$ emitted by atoms in the particular volume which is imaged onto the slits of our monochromator. This is given by the following:

$$\begin{aligned} I_{nl_j \rightarrow n'l'_j} &= \int_{\text{Vol}} I_{nl_j \rightarrow n'l'_j}(\vec{r}) d^3r \\ &= \frac{hc}{\lambda_{nl_j \rightarrow n'l'_j}} \varepsilon_{nl_j \rightarrow n'l'_j} \frac{d\Omega}{4\pi} \\ &\quad \times \Gamma_{nl_j \rightarrow n'l'_j}^{\text{nat}} T_{nl_j \rightarrow n'l'_j} \int_{\text{Vol}} n_{nl_j}(\vec{r}) d^3r \\ &= \frac{hc}{\lambda_{nl_j \rightarrow n'l'_j}} \varepsilon_{nl_j \rightarrow n'l'_j} \frac{d\Omega}{4\pi} \Gamma_{nl_j \rightarrow n'l'_j}^{\text{nat}} \\ &\quad \times T_{nl_j \rightarrow n'l'_j} \frac{k_{nl_j} \tau_{nl_j}^{\text{eff}}}{2} \int_{\text{Vol}} [n_{6P_j}(\vec{r})]^2 d^3r. \end{aligned} \quad (4)$$

Here $hc/\lambda_{nl_j \rightarrow n'l'_j}$ is the energy of a fluorescence photon ($\lambda_{nl_j \rightarrow n'l'_j}$ is the transition wavelength), $\Gamma_{nl_j \rightarrow n'l'_j}^{\text{nat}}$ is the natural radiative rate of the transition, $\varepsilon_{nl_j \rightarrow n'l'_j}$ is the detection system efficiency (including effects due to the photomultiplier, monochromator grating, and any filters used) at the frequency of interest, and $d\Omega/4\pi$ is the probability that the fluorescent photon is emitted into the finite collection solid angle of the detection system. Here we have assumed that collisions and radiation trapping quickly destroy any atomic alignment or orientation, and thus the emissions are isotropic. Finally, $T_{nl_j \rightarrow n'l'_j}$ is the average probability that the photon emitted in the detection direction will pass through the vapor between its point of origin and the cell walls without being absorbed. This probability depends on the distribution of both the nl_j and $n'l'_j$ atoms in the vapor as well as on the details of the transition line shape. The calculation of $T_{nl_j \rightarrow n'l'_j}$ will be described in Sec. II B.

Factors such as the absolute detection efficiency and collection solid angle are experimentally difficult to determine. Therefore it is advantageous to measure fluorescence ratios. Specifically, we measure the ratio of fluorescence from the state nl_j , populated through energy pooling, to fluorescence observed on the directly pumped resonance transition; i.e., on the $6P_J \rightarrow 6S_{1/2}$ transition

$$\begin{aligned} \frac{I_{nl_j \rightarrow n'l'_j}}{I_{6P_J \rightarrow 6S_{1/2}}} &= \frac{\lambda_{6P_J \rightarrow 6S_{1/2}}}{\lambda_{nl_j \rightarrow n'l'_j}} \frac{\varepsilon_{nl_j \rightarrow n'l'_j}}{\varepsilon_{6P_J \rightarrow 6S_{1/2}}} \frac{\Gamma_{nl_j \rightarrow n'l'_j}^{\text{nat}}}{\Gamma_{6P_J \rightarrow 6S_{1/2}}^{\text{nat}}} \\ &\quad \times \frac{T_{nl_j \rightarrow n'l'_j}}{T_{6P_J \rightarrow 6S_{1/2}}} \frac{k_{nl_j} \tau_{nl_j}^{\text{eff}}}{2} \frac{\int [n_{6P_j}(\vec{r})]^2 d^3r}{\int n_{6P_j}(\vec{r}) d^3r}. \end{aligned} \quad (5)$$

Finally, we can solve Eq. (5) for the rate coefficient k_{nl_j}

$$\begin{aligned} k_{nl_j} &= \left(\frac{I_{nl_j \rightarrow n'l'_j} / \varepsilon_{nl_j \rightarrow n'l'_j}}{I_{6P_J \rightarrow 6S_{1/2}} / \varepsilon_{6P_J \rightarrow 6S_{1/2}}} \right) \\ &\quad \times \frac{\lambda_{nl_j \rightarrow n'l'_j}}{\lambda_{6P_J \rightarrow 6S_{1/2}}} \frac{\Gamma_{6P_J \rightarrow 6S_{1/2}}^{\text{nat}}}{\Gamma_{nl_j \rightarrow n'l'_j}^{\text{nat}}} \frac{T_{6P_J \rightarrow 6S_{1/2}}}{T_{nl_j \rightarrow n'l'_j}} \frac{2}{\tau_{nl_j}^{\text{eff}}} \\ &\quad \times \frac{\int n_{6P_j}(\vec{r}) d^3r}{\int [n_{6P_j}(\vec{r})]^2 d^3r}. \end{aligned} \quad (6)$$

In the present experiment, the detection volume is a thin strip of height $\Delta y \sim 150 \mu\text{m}$ oriented along the z (laser propagation) axis [see Fig. 2(b)]. If we assume that the excitation is uniform along the z axis, and because Δy is small, we write the volume integrals in Cartesian coordinates, and immediately carry out the integrations over y and z

$$\begin{aligned} k_{nl_j} &= \left(\frac{I_{nl_j \rightarrow n'l'_j} / \varepsilon_{nl_j \rightarrow n'l'_j}}{I_{6P_J \rightarrow 6S_{1/2}} / \varepsilon_{6P_J \rightarrow 6S_{1/2}}} \right) \\ &\quad \times \frac{\lambda_{nl_j \rightarrow n'l'_j}}{\lambda_{6P_J \rightarrow 6S_{1/2}}} \frac{\Gamma_{6P_J \rightarrow 6S_{1/2}}^{\text{nat}}}{\Gamma_{nl_j \rightarrow n'l'_j}^{\text{nat}}} \frac{T_{6P_J \rightarrow 6S_{1/2}}}{T_{nl_j \rightarrow n'l'_j}} \\ &\quad \times \frac{2}{(\tau_{nl_j}^{\text{eff}} / \tau_{nl_j}^{\text{nat}})} \frac{\int_{-R}^R n_{6P_j}(x) dx}{\int_{-R}^R [n_{6P_j}(x)]^2 dx}, \end{aligned} \quad (7)$$

where R is the cell radius. Note that, in this expression, $\Gamma_{nl_j \rightarrow n'l'_j}^{\text{nat}} \tau_{nl_j}^{\text{nat}}$ is the branching ratio for the $nl_j \rightarrow n'l'_j$ transition, and $(\tau_{nl_j}^{\text{eff}} / \tau_{nl_j}^{\text{nat}})$ is a factor which characterizes the effect of radiation trapping on the nl_j state lifetime.

B. Radiation trapping and optical depth effects

Because of the high density of ground-state atoms and the strength of the resonance transitions, it is unlikely that resonance photons can escape the cell without being reabsorbed. Thus the excitation lives longer in the vapor than one natural excited-state lifetime. There are two major effects of radiation trapping in the present context. The spatial distribution of excited atoms is different than the distribution initially

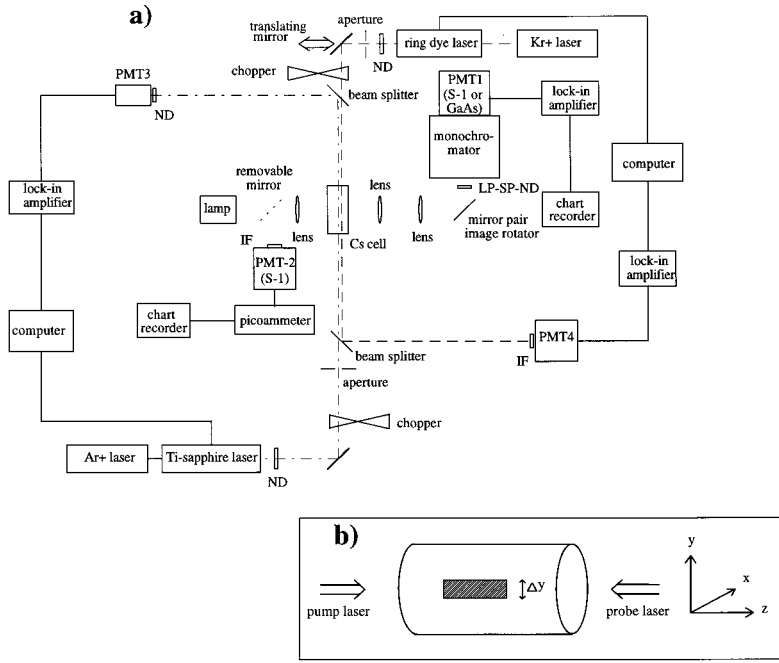


FIG. 2. (a) Experimental setup. The Ti:sapphire laser was used to pump the $6S_{1/2} \rightarrow 6P_J$ transition. The monochromator and photomultiplier tube 1 (PMT-1) were used to spectrally resolve the cesium atomic line fluorescence. PMT-2 was used to monitor total resonance line (D_1 or D_2) fluorescence, and PMT-3 monitored the transmission of the Ti:sapphire beam through the cell. The ring dye laser was used to probe the $6P_J$ level density at various positions in the cell (determined by the position of the translating mirror). PMT-4 was used to monitor the dye laser transmission. IF, LP, SP, and ND represent interference, long-pass, short-pass and neutral density filter, respectively. (b) insert showing the cell geometry and the region from which fluorescence was detected.

produced by the pump laser, and the effective lifetime of the excited atoms (and hence the time in which they can undergo energy-pooling collisions) is lengthened over the natural radiative lifetime. Both of these effects are properly taken into account in Eq. (7), which uses calculated effective lifetimes and transmission factors, and spatial integrals over the measured steady-state distribution of excited atoms.

The normalized transmission factors in Eq. (7) are defined as follows:

$$T_{nl_{J'} \rightarrow n'l'_{J''}} = \frac{\int_{\text{Vol}} n_{nl_{J'}}(\vec{r}) P_{nl_{J'} \rightarrow n'l'_{J''}}^{\text{escape}}(\vec{r}) d^3r}{\int_{\text{Vol}} n_{nl_{J'}}(\vec{r}) d^3r} = \frac{\int_{-R}^R n_{nl_{J'}}(x) P_{nl_{J'} \rightarrow n'l'_{J''}}^{\text{escape}}(x) dx}{\int_{-R}^R n_{nl_{J'}}(x) dx}, \quad (8)$$

where our specific detection system geometry, described above Eq. (7), has been used in the last step. The escape factor $P_{nl_{J'} \rightarrow n'l'_{J''}}^{\text{escape}}(x)$ is the probability that $nl_{J'} \rightarrow n'l'_{J''}$ photons emitted at position x can escape the cell in the detection direction through the vapor path length $(R-x)$ without being reabsorbed

$$P_{nl_{J'} \rightarrow n'l'_{J''}}^{\text{escape}}(x) = \int \sigma_{nl_{J'} \leftarrow n'l'_{J''}}(\omega) \exp\left[-\sigma_{nl_{J'} \leftarrow n'l'_{J''}}(\omega) \int_x^R n_{n'l'_{J''}}(x') dx'\right] d\omega \Big/ \int \sigma_{nl_{J'} \leftarrow n'l'_{J''}}(\omega) d\omega. \quad (9)$$

Here $\sigma_{nl_{J'} \leftarrow n'l'_{J''}}(\omega)$ is the absorption cross section at angular frequency ω . Thus, $\sigma_{nl_{J'} \leftarrow n'l'_{J''}}(\omega) / \int \sigma_{nl_{J'} \leftarrow n'l'_{J''}}(\omega) d\omega$ is the normalized probability that a photon of frequency ω will be emitted at any position x , and $\exp[-\sigma_{nl_{J'} \leftarrow n'l'_{J''}}(\omega) \int_x^R n_{n'l'_{J''}}(x') dx']$ is the probability that the photon of frequency ω emitted at x can escape through the (possibly nonuniform) distribution of lower-state atoms $n_{n'l'_{J''}}(x')$ and reach the cell wall a distance $(R-x)$ away. For a line with hyperfine structure, the absorption coefficients add; $k_{nl_{J'} \leftarrow n'l'_{J''}}(\omega) = \sum_F \sum_{F'} k_{nl_{J'}(F) \leftarrow n'l'_{J''}(F')}(\omega) = \sum_F \sum_{F'} \sigma_{nl_{J'}(F) \leftarrow n'l'_{J''}(F')}(\omega) n_{n'l'_{J''}(F')}$. Thus if we assume that the lower-state hyperfine levels are populated statistically, we may define a line-shape factor $\sigma_{nl_{J'} \leftarrow n'l'_{J''}}(\omega)$ for the full transition

$$\sigma_{nl_{J'} \leftarrow n'l'_{J''}}(\omega) \equiv \frac{k_{nl_{J'} \leftarrow n'l'_{J''}}(\omega)}{n_{n'l'_{J''}}} = \sum_F \sum_{F'} \sigma_{nl_{J'}(F) \leftarrow n'l'_{J''}(F')}(\omega) \frac{g(F')}{\sum_{F'} g(F')}, \quad (10)$$

where $g(F') = 2F' + 1$ is the statistical weight of level $n'l'_{J''}(F')$. Finally, the absorption cross sections for individual hyperfine transitions are each given by a Voigt function of the form

$$\sigma_{nl_{J'}(F) \leftarrow n'l'_{J''}(F')}(\omega) = \frac{\lambda^2}{8\pi} \frac{g(F)}{g(F')} \frac{\Gamma_{nl_{J'} \rightarrow n'l'_{J''}} \Gamma_{nl_{J'} \rightarrow n'l'_{J''}}^{\text{nat}}}{\pi^{1/2} \Delta} \times \int_{-\infty}^{\infty} d\omega' \frac{\exp[-(\omega' - \omega_{nl_{J'}(F) \rightarrow n'l'_{J''}(F')})^2 / \Delta^2]}{(\omega - \omega')^2 + (\Gamma_{nl_{J'} \rightarrow n'l'_{J''}} / 2)^2}, \quad (11)$$

where $\Gamma_{nl_{j'} \rightarrow n'l'_{j''}}$ is the Lorentzian linewidth [full width at half maximum (FWHM) in angular frequency units], $\Delta = 1/\lambda \sqrt{2kT/m}$ is the Gaussian (Doppler) linewidth (full width at $1/e$ maximum in angular frequency units), and $\omega_{nl_{j'}(F) \rightarrow n'l'_{j''}(F')}$ is the line-center frequency of the $nl_{j'}(F) \rightarrow n'l'_{j''}(F')$ transition. k is Boltzmann's constant, T is the absolute temperature, and m is the cesium atomic mass. Thus the normalized transmission factors $T_{nl_{j'} \rightarrow n'l'_{j''}}$ in Eq. (7) can be calculated for any transition from Eqs. (8)–(11) if the hyperfine structure and Lorentzian linewidth of the transition, and the spatial distribution of the lower-state $n'l'_{j''}$ atoms is known. The only significant assumption that has been made is that the lower-state hyperfine levels are populated in a statistical ratio. This assumption will be discussed further below. For each hyperfine transition of the various $nl_{j'} \rightarrow n'l'_{j''}$ and $6P_{j'} \rightarrow 6S_{1/2}$ transitions of interest, and at each temperature, we calculate $\sigma_{nl_{j'}(F) \leftarrow n'l'_{j''}(F')}(\omega)$ as a function of frequency using the Voigt algorithm of Refs. [22] and [23] (see also [24]).

Note that we have not taken optical pumping into account when discussing the $6P_{j'} \rightarrow 6S_{1/2}$ transmission factor. Since the pump laser we use is single mode, with a linewidth which is small compared to the ground-state hyperfine splitting of 9.193 GHz, we pump atoms almost exclusively from one hyperfine component. Due to optical pumping, atoms will tend to accumulate in the other (unpumped) hyperfine level. For example, if we pump the $6S_{1/2}(F=4) \rightarrow 6P_{1/2}(F'=4)$ transition, atoms will accumulate in the $6S_{1/2}(F=3)$ level. Consequently, reabsorption of photons at the $6P_{1/2} \rightarrow 6S_{1/2}(F=3)$ transition frequency will be much more severe than for those at the $6P_{1/2} \rightarrow 6S_{1/2}(F=4)$ frequency. However, this optical pumping only occurs within the pump laser column which is surrounded by a much larger volume of ground-state atoms where the ratio of hyperfine level populations is approximately statistical. The transmission factor is determined primarily by these atoms outside the laser column. Thus we believe that use of a transmission factor based on a statistical distribution of atoms in the $6S_{1/2}$ hyperfine levels is justified. However, this assumption of a statistical ratio of ground-state hyperfine level populations used in these calculations is a significant source of uncertainty in our analysis.

From Eq. (7) it can be seen that the effective lifetime of the state $nl_{j'}$ is also needed in order to determine the energy-pooling rate coefficient $k_{nl_{j'}}$. In the present context, collisional quenching of $nl_{j'}$ atoms can be neglected. However, due to radiation trapping,

$$\begin{aligned} \tau_{nl_{j'}}^{\text{eff}} &= \left[\sum_{n'l'_{j''}} \Gamma_{nl_{j'} \rightarrow n'l'_{j''}}^{\text{eff}} \right]^{-1} \\ &= \left[\sum_{n'l'_{j''}} g_{nl_{j'} \rightarrow n'l'_{j''}} \Gamma_{nl_{j'} \rightarrow n'l'_{j''}}^{\text{nat}} \right]^{-1}, \end{aligned} \quad (12)$$

where $\Gamma_{nl_{j'} \rightarrow n'l'_{j''}}^{\text{eff}}$ is the effective radiative rate (and $g_{nl_{j'} \rightarrow n'l'_{j''}}$ is the escape factor) of the transition.

Radiation trapping has been studied extensively for Doppler broadened alkali resonance lines [25–28]. Effective radiative rates can be calculated accurately using the Holstein

[29–30] and Milne [31] theories in the limits $k_0 l \gg 10$ and $k_0 l \leq 10$, respectively, as has been shown in Refs. [26] and [28]. Here k_0 is the line-center absorption coefficient, and l is the effective escape distance. However, to model the results of the present experiment, we use the Molisch *et al.* theory of radiation trapping [32,33] (see also Ref. [34]) which reduces to the Holstein and Milne results in the appropriate limits. The most severe, and in the context of the present experiment most significant, trapping occurs on the $6P_{j'} \rightarrow 6S_{1/2}$ resonance transition. However, these trapping effects are all included in the transmission factor $T_{6P_{j'} \rightarrow 6S_{1/2}}$. The $7P_{j'} \rightarrow 6S_{1/2}$ transitions are the only transitions to the ground state for which we must calculate effective radiative rates.

According to the general formulation of Holstein [29,30], Payne and Cook [35], and van Trigt [36], for certain geometries, the steady-state excited-atom spatial distribution $n(\vec{r})$ can be expanded in a series of orthogonal eigenmodes $n(\vec{r}) = \sum_j a_j n_j(\vec{r})$. Each eigenmode is a mathematical solution of the radiation diffusion equation characterized by a single exponential decay rate $\beta_j = g_j \Gamma^{\text{nat}}$. Here, g_j is the escape factor for mode j , and Γ^{nat} is the natural radiative rate for the excited state. Note that the individual eigenmode solutions are nonphysical, since (except for the fundamental mode) each has regions of negative amplitude (see, for example, Figs. 1 and 2 of Ref. [36]). Nevertheless, these eigenmodes form a complete set, and any actual excited-atom spatial distribution can be expanded as a linear superposition of them.

We model our cell as a cylinder of radius $R = 1.05$ cm and length L , with $L \gg R$. In this experiment we measure the cylindrically symmetric steady-state excited-atom spatial distribution $n_{6P_{j'}}(r)$, and we assume that the $7P_{j'}$ density is proportional to $[n_{6P_{j'}}(r)]^2$ according to Eq. (3). Thus we can calculate the mode amplitudes from

$$a_j = \int_0^R [n_{6P_{j'}}(r)]^2 n_j(r) r dr \bigg/ \int_0^R [n_{6P_{j'}}(r)]^2 r dr. \quad (13)$$

Finally, the effective radiative rate $\Gamma_{7P_{j'} \rightarrow 6S_{1/2}}^{\text{eff}}$, or escape factor $g_{7P_{j'} \rightarrow 6S_{1/2}}$, is given by a weighted average of the decay rates for the individual eigenmodes

$$\begin{aligned} \Gamma_{7P_{j'} \rightarrow 6S_{1/2}}^{\text{eff}} &= g_{7P_{j'} \rightarrow 6S_{1/2}} \Gamma_{7P_{j'} \rightarrow 6S_{1/2}}^{\text{nat}} \\ &= \frac{\Gamma_{7P_{j'} \rightarrow 6S_{1/2}}^{\text{nat}} \sum_j g_j a_j \int n_j(r) d^3 r}{\sum_j a_j \int n_j(r) d^3 r} \\ &= \frac{\Gamma_{7P_{j'} \rightarrow 6S_{1/2}}^{\text{nat}} \sum_j g_j a_j \int_0^R n_j(r) r dr}{\sum_j a_j \int_0^R n_j(r) r dr}. \end{aligned} \quad (14)$$

In the present work, we model our results using the Molisch theory of radiation trapping [32,33]. This theory is based upon numerical integration of the Holstein radiation diffusion equation and yields analytic fitting equations for the escape factors and eigenmodes. Most important, Molisch *et al.* give escape factors for the ten lowest eigenmodes which allows an accurate expansion of the excited-atom spatial profile in Eq. (14). In this case, where the radiation trap-

ping is dominated by the Doppler core of the line, the escape factor for the j th mode is given according to Molisch *et al.* [33] by the expression

$$g_j^D = \left[1 + \frac{1}{m_j^D} k_0 R \sqrt{\ln([k_0 R/2] + e)} - \frac{c_{0j}^D k_0 R \ln(k_0 R) + c_{1j}^D k_0 R + c_{2j}^D (k_0 R)^2}{1 + c_{3j}^D k_0 R + c_{4j}^D (k_0 R)^2} \right]^{-1}. \quad (15)$$

The coefficients m_j^D and c_{ij}^D for the first ten modes are tabulated in Table 1 of Ref. [33] (the superscript D stands for Doppler line shape), and $k_0 R$ is the line-center opacity. Note that the escape factor g_j^D used here is the inverse of the Molisch trapping factor g defined in Ref. [33].

To calculate $\Gamma_{7P_{J'} \rightarrow 6S_{1/2}}^{\text{eff}}$ we first determined the Molisch Doppler line-shape cylinder eigenfunctions as described in Ref. [33] (see also Ref. [34]). We then calculated the mode amplitudes of the experimentally measured excited-atom spatial distribution $n_{7P_{J'}}(\vec{r}) \propto [n_{6P_J}(\vec{r})]^2$ using Eq. (13). This information was used in Eq. (14), along with the lowest ten mode escape factors from Eq. (15), to calculate the radiative escape factor of each hyperfine transition.

In our use of Eq. (15) for lines with *unresolved* hyperfine structure, we replace the line-center optical depth $k_0 R$, calculated for the line without structure, by $k_{\text{max}} R$, where k_{max} is the maximum absorption coefficient for the line with structure (see Refs. [26], [28], and [37]). The latter is the lower state density times the maximum absorption cross section of the composite line from Eq. (10). In the case of the $7P_{J'} \rightarrow 6S_{1/2}$ transitions, the lower-state hyperfine structure is well resolved, but the upper-state structure is not. Thus we calculate

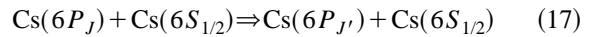
$$\Gamma_{7P_{J'} \rightarrow 6S_{1/2}}^{\text{eff}} = g_{7P_{J'} \rightarrow 6S_{1/2}(F=3)} \Gamma_{7P_{J'} \rightarrow 6S_{1/2}(F=3)}^{\text{nat}} + g_{7P_{J'} \rightarrow 6S_{1/2}(F=4)} \Gamma_{7P_{J'} \rightarrow 6S_{1/2}(F=4)}^{\text{nat}}, \quad (16)$$

where we consider the upper-state hyperfine levels to be populated in statistical equilibrium by the energy-pooling process. Values of $\Gamma_{7P_{J'} \rightarrow 6S_{1/2}}^{\text{eff}}$ calculated using the procedure described above are used to determine $\tau_{7P_{J'}}^{\text{eff}}/\tau_{7P_{J'}}^{\text{nat}}$, and these are listed in Table I where the results are presented.

Under our conditions, radiative rates are reduced by trapping by less than 45% for the $7P_{1/2} \rightarrow 6S_{1/2}$ transition, but by as much as 90% for the $7P_{3/2} \rightarrow 6S_{1/2}$ transition, using the natural radiative rates of Warner [38]. However, values of $\tau_{7P_{J'} \rightarrow 6S_{1/2}}^{\text{eff}}$ differ from $\tau_{7P_{J'} \rightarrow 6S_{1/2}}^{\text{nat}}$ by 70% in the most extreme case.

Finally, with strong pumping we must worry about trapping on transitions which terminate on the $6P_J$ levels. These transitions, which include $8S_{1/2} \rightarrow 6P_J$ and $6D_{J'} \rightarrow 6P_J$, are of sufficiently low optical depth under the conditions of the present experiment that we treat them using the Molisch theory, but retain only the fundamental mode of the expansion. The $6P_J$ level populations are not uniformly distributed in space since the pump excitation is not uniform. However we measure the spatial distribution of the laser excited $6P_J$ atoms (see Sec. III). Therefore we can estimate an effective escape radius for photons resonant with these transitions.

The hyperfine levels of $6P_{1/2}$ are sufficiently separated in energy that transitions to $6P_{1/2}(F'=3)$ and $6P_{1/2}(F'=4)$ are treated separately. The hyperfine level separation in the $6P_{3/2}$ state is much smaller, however, and we treat transitions to $6P_{3/2}$ as a composite line as discussed above. Trapping corrections of this type reduce the effective radiative rates by up to 80%, but are typically less than 60% for the $6D_{J'} \rightarrow 6P_J$ transitions and always less than 6% for the $8S_{1/2} \rightarrow 6P_J$ transition where $6P_J$ is the level pumped by the laser. Again, the effects on $\tau_{nl_{J'}}^{\text{eff}}$ are typically less than those on the effective radiative rates; <26% except in two cases (see Table I) for $nl_{J'} = 6D_{3/2,5/2}$ and <2% for $nl_{J'} = 8S_{1/2}$. Note that trapping on transitions terminating on the fine-structure level $6P_{J'}$, which is not directly populated by the laser is generally quite small, since fine-structure level changing collisions



are relatively rare at the densities of this experiment. Trapping on transitions which terminate on levels other than $6S_{1/2}$ and $6P_J$ can always be neglected.

III. THE EXPERIMENT

A. Setup and fluorescence measurements

The experimental setup is shown in Fig. 2. Cesium metal is contained in a cylindrical Pyrex cell (Environmental Optical Sensors, Inc.) of inner length 7.0 cm and inner radius 1.05 cm. The cell is contained in a cross-shaped brass oven (not shown in the figure), with four quartz windows, which is heated with resistive heater tapes. Three thermocouples are attached to the cell in order to monitor temperature. Typically the three temperatures agree to within 5–6 °C, and are constant to within 2 °C over the course of a set of measurements. The liquid cesium metal can be seen to sit at the site where the coldest temperature is registered.

The density of cesium atoms in the vapor phase is calculated from the Nesmeyanov vapor pressure formula [39]. At room temperature, the various hyperfine components of the cesium D_1 line are optically thin. Thus the line-center absorption coefficient can be used to obtain an accurate value for the atom density at that temperature. We find that the value obtained in this manner is larger than the Nesmeyanov value by 4.5%. Since this corresponds to a temperature discrepancy of only 1/2 °C (which is equal to the uncertainty in our temperature measurement), we assume that the Nesmeyanov curve is fairly accurate in this temperature range. We estimate that ground-state densities obtained in this manner are accurate to ~5–10% in the temperature range 23–92 °C.

The cesium atoms are excited to particular hyperfine components of the $6P_{1/2}$ and $6P_{3/2}$ states using a single-mode Ti:Sapphire laser (Coherent model 899-29, pumped by 10 W all lines from an argon-ion laser). Typical Ti:Sapphire laser power was 580 mW at the D_1 line and 650 mW at the D_2 line. Laser linewidth was ~1 MHz. Although several excitation geometries were tried, our most accurate data were taken with the Ti:Sapphire laser (hereafter called the pump laser) gently focused into the cell using a 4 m focal length lens. A 2.03 mm aperture just before the entrance window was used to better approximate a top-hat spatial profile, which was

TABLE I. Measured rate coefficients for the cesium energy-pooling collisions $\text{Cs}(6P_J) + \text{Cs}(6P_J) \rightarrow \text{Cs}(nI_{J'}) + \text{Cs}(6S_{1/2})$. Note: $\Gamma_{6P_{1/2} \rightarrow 6S_{1/2}}^{\text{nat}} = 2.89 \times 10^7 \text{ s}^{-1}$ and $\Gamma_{6P_{3/2} \rightarrow 6S_{1/2}}^{\text{nat}} = 3.26 \times 10^7 \text{ s}^{-1}$ from Warner [38].

$nI_{J'}$	Temp (°C)	$n_{6S_{1/2}}$ (10^{12} cm^{-3})	$T_{6P_{3/2} \rightarrow 6S_{1/2}}$	$\int_{-R}^R n_{6P_{3/2}}(x) dx$ $\int_{-R}^R [n_{6P_{3/2}}(x)]^2 dx$	Monitored Transition $nI_{J'} \rightarrow n'I_{J''}$	$\frac{I_{nI_{J'} \rightarrow n'I_{J''}} / \epsilon_{nI_{J'} \rightarrow n'I_{J''}}}{I_{6P_{3/2} \rightarrow 6S_{1/2}} / \epsilon_{6P_{3/2} \rightarrow 6S_{1/2}}}$	$\Gamma_{nI_{J'} \rightarrow n'I_{J''}}^{\text{nat}}$ (s^{-1})	$T_{nI_{J'} \rightarrow n'I_{J''}}$	$\tau_{nI_{J'}}^{\text{nat}}$ (s)	$\frac{\tau_{nI_{J'}}^{\text{eff}}}{\tau_{nI_{J'}}^{\text{nat}}}$	$k_{nI_{J'}}$ ($\text{cm}^3 \text{ s}^{-1}$)
$7P_{1/2}$	64	1.25	0.0249	$(3.88 \times 10^{10})^{-1}$	$7P_{1/2} \rightarrow 6S_{1/2}$	2.69×10^{-8}	1.58×10^6	0.934	1.55×10^{-7}	1.02	2.59×10^{-12}
	74	2.62	0.0109	$(1.01 \times 10^{11})^{-1}$		2.06×10^{-7}		0.862		1.04	3.54×10^{-12}
	74	2.62	0.0130	$(1.62 \times 10^{11})^{-1}$		8.73×10^{-7}		0.883		1.04	1.09×10^{-11}
	85	5.62	0.00548	$(4.44 \times 10^{11})^{-1}$		2.14×10^{-6}		0.739		1.08	4.73×10^{-12}
	85	5.62	0.00607	$(4.27 \times 10^{11})^{-1}$		2.57×10^{-6}		0.749		1.08	6.45×10^{-12}
	91.5	8.63	0.00440	$(8.23 \times 10^{11})^{-1}$		6.71×10^{-6}		0.627		1.12	7.34×10^{-12}
	92	8.92	0.00424	$(5.42 \times 10^{11})^{-1}$		3.69×10^{-6}		0.627		1.12	5.88×10^{-12}
	64	1.25	0.0249	$(3.88 \times 10^{10})^{-1}$	$7P_{3/2} \rightarrow 6S_{1/2}$	3.12×10^{-8}	4.18×10^6	0.689	1.10×10^{-7}	1.22	1.81×10^{-12}
	74	2.62	0.0109	$(1.01 \times 10^{11})^{-1}$		2.35×10^{-7}		0.465		1.38	2.99×10^{-12}
	74	2.62	0.0130	$(1.62 \times 10^{11})^{-1}$		8.64×10^{-7}		0.523		1.38	7.29×10^{-12}
$7P_{3/2}$	85	5.62	0.00548	$(4.44 \times 10^{11})^{-1}$		2.11×10^{-6}		0.236		1.60	5.25×10^{-12}
	85	5.62	0.00607	$(4.27 \times 10^{11})^{-1}$		2.46×10^{-6}		0.254		1.59	6.56×10^{-12}
	91.5	8.63	0.00440	$(8.23 \times 10^{11})^{-1}$		6.22×10^{-6}		0.137		1.68	1.09×10^{-11}
	92	8.92	0.00424	$(5.42 \times 10^{11})^{-1}$		2.89×10^{-6}		0.132		1.70	7.62×10^{-12}
	64	1.25	0.0249	$(3.88 \times 10^{10})^{-1}$	$6D_{3/2} \rightarrow 6P_{1/2}$	2.62×10^{-6}	9.86×10^6	1.00	7.92×10^{-8}	1.01	1.43×10^{-10}
	74	2.62	0.0109	$(1.01 \times 10^{11})^{-1}$		8.07×10^{-6}		0.996		1.02	7.34×10^{-11}
	74	2.62	0.0130	$(1.62 \times 10^{11})^{-1}$		1.42×10^{-5}		0.994		1.03	9.53×10^{-11}
	85	5.62	0.00548	$(4.44 \times 10^{11})^{-1}$		8.52×10^{-5}		0.962		1.07	8.78×10^{-11}
	85	5.62	0.00607	$(4.27 \times 10^{11})^{-1}$		3.97×10^{-5}		0.988		1.06	4.61×10^{-11}
	91.5	8.63	0.00440	$(8.23 \times 10^{11})^{-1}$		2.08×10^{-4}		0.904		1.19	8.89×10^{-11}
$6D_{3/2}$	92	8.92	0.00424	$(5.42 \times 10^{11})^{-1}$		1.43×10^{-4}		0.957		1.07	9.38×10^{-11}
	92	8.92	0.00424	$(5.42 \times 10^{11})^{-1}$	$6D_{3/2} \rightarrow 6P_{3/2}$	2.95×10^{-5}	2.67×10^6	0.767	7.92×10^{-8}	1.07	9.37×10^{-11}
	92	8.92	0.00424	$(5.42 \times 10^{11})^{-1}$	$6D_{5/2} \rightarrow 6P_{3/2}$	2.05×10^{-4}	1.49×10^7	0.244	6.68×10^{-8}	2.44	1.89×10^{-10}
	92	8.92	0.00424	$(5.42 \times 10^{11})^{-1}$	$4F_{5/2} \rightarrow 5D_{3/2}$	1.80×10^{-5}	2.26×10^7	1.00	3.88×10^{-8}	1.00	1.23×10^{-11}
	92	8.92	0.00424	$(5.42 \times 10^{11})^{-1}$	$4F_{7/2} \rightarrow 5D_{5/2}$	3.15×10^{-5}	2.03×10^7	1.00	4.61×10^{-8}	1.00	2.04×10^{-11}
	74	2.62	0.0130	$(1.62 \times 10^{11})^{-1}$	$8S_{1/2} \rightarrow 6P_{1/2}$	7.79×10^{-7}	1.97×10^6	1.00	1.05×10^{-7}	1.01	1.74×10^{-11}
	85	5.62	0.00607	$(4.27 \times 10^{11})^{-1}$		3.10×10^{-6}		1.00		1.03	1.21×10^{-11}
	92	8.92	0.00424	$(5.42 \times 10^{11})^{-1}$		1.12×10^{-5}		0.998		1.02	2.42×10^{-11}
	85	5.62	0.00607	$(4.27 \times 10^{11})^{-1}$	$8S_{1/2} \rightarrow 6P_{3/2}$	3.39×10^{-6}	3.62×10^6	0.977	1.05×10^{-7}	1.03	7.67×10^{-12}
	92	8.92	0.00424	$(5.42 \times 10^{11})^{-1}$		2.08×10^{-5}		0.980		1.02	2.60×10^{-11}

measured at the position of the center of the cell using a two-dimensional charge-coupled-device (CCD) array (SpectraSource Instruments LYNXX PC Plus). The beam diameter at the cell center was found to be ~ 1.3 mm under these conditions.

The pump laser could be tuned to particular hyperfine transitions of either the D_1 or D_2 line of cesium. For D_1 line excitation, the full hyperfine structure of both upper and lower states is well resolved. However, for D_2 excitation, the upper-state hyperfine splittings are smaller than the Doppler widths. Thus we pump a combination of upper hyperfine levels; either $6S_{1/2}(F=3) \rightarrow 6P_{3/2}(F'=2,3,4)$ or $6S_{1/2}(F=4) \rightarrow 6P_{3/2}(F'=3,4,5)$. Optical pumping of the ground-state hyperfine levels reduces the number of atoms that can be pumped to the excited state. However, this is not a problem in the present work since the density and spatial distribution of excited atoms is directly measured.

Transmission of the pump-laser beam through the cell was monitored using photomultiplier PMT3 (Hamamatsu model R406) (see Fig. 2). At the lower densities studied in this work, the attenuation of the laser beam along the length of the cell could generally be neglected even when the laser was tuned directly to resonance. However, at high density, absorption at line center of a particular hyperfine transition caused severe attenuation of the laser beam before it reached the observation region at the center of the cell. In either case, we set the laser frequency to maximize $6P_J \rightarrow 6S_{1/2}$ fluorescence from the observation region. At higher densities this meant that the laser frequency was slightly detuned from line center, so that again the attenuation could generally be neglected. Thus the density of excited atoms could be considered to be independent of z [see Fig. 2(b)]. This turns out to be a very good approximation at our low densities, and is still reasonable at the higher densities.

A pair of lenses and an image rotator were used to image fluorescence onto the slits of a 0.22 m monochromator (Spex model 1681) with 1200 groove/mm grating blazed at 500 nm. With 300 μm slits (providing a spectral resolution of ~ 1 nm) and 1:2 imaging, the volume from which fluorescence was collected was a strip of width $\Delta y \sim 150$ μm and length 0.5 cm oriented along the laser propagation (z) axis. A GaAs (Hamamatsu model R636) photomultiplier tube (PMT1) was used to detect the resolved $6P_{1/2} \rightarrow 6S_{1/2}$, $6P_{3/2} \rightarrow 6S_{1/2}$, $7P_{1/2} \rightarrow 6S_{1/2}$, $7P_{3/2} \rightarrow 6S_{1/2}$, and $6D_{3/2} \rightarrow 6P_{1/2}$ fluorescence on each data run. An S-1 PMT (Hamamatsu model R-406) replaced the GaAs tube for one data run at 92 °C to record near-infrared $4F_{7/2} \rightarrow 5D_{5/2}$, $4F_{5/2} \rightarrow 5D_{3/2}$, $6D_{5/2} \rightarrow 6P_{3/2}$, and $6D_{3/2} \rightarrow 6P_{3/2,1/2}$ fluorescence, in order to obtain $4F_{J'}$ and $6D_{5/2}$ energy-pooling rates relative to the more systematically studied $7P_{J'}$ and $6D_{3/2}$ rates. $8S_{1/2} \rightarrow 6P_J$ fluorescence was also recorded using either PMT on a few runs. The pump laser was chopped, and the PMT signals were processed by a lock-in amplifier and displayed on a chart recorder.

A long-pass filter (either Schott RG-610 or RG-695) was placed in front of the monochromator entrance slits for all but the $7P \rightarrow 6S$ fluorescence to eliminate 2nd order scattering from the grating. A short-pass filter (Reynard 942 or 944, with cut-on wavelength of 675 or 700 nm, respectively) was used to block scattered D_1 and D_2 line fluorescence (which could otherwise leak through the monochromator) when recording the $7P$ fluorescence. Neutral density filters were

used to attenuate the strong D_1 and D_2 line signals so that they could be recorded using the same monochromator slits and PMT voltage. The wavelength-dependent relative detection system efficiency, including the effects of all filters, was measured using a calibrated tungsten-halogen lamp [40]. A free-standing photomultiplier (PMT2-Hamamatsu R406 or R636) was used with either a D_1 or D_2 line interference filter to monitor the resonance line radiation (see Fig. 2). This allowed constant monitoring to guard against frequency or power drift of the pump laser.

B. Measurement of the excited atom density and spatial distribution

A single-mode cw dye laser (Coherent 699-29, using LD-700 dye pumped by a 6 W krypton ion laser) was used to probe the density and spatial distribution of the atoms excited to the $6P_J$ levels. The probe-laser power was reduced to typically 10–100 nW using neutral density filters, and the probe beam diameter was reduced to 0.75 mm or less at the center of the cell using a 1 m focal length lens and an aperture. Both pump- and probe-laser beams were well collimated over the length of the cesium cell.

The probe beam could be moved spatially across the cell diameter using the mirror mounted on the translation stage shown in Fig. 2. The probe laser frequency was scanned across the various hyperfine transitions of either the $6P_{3/2} \rightarrow 7D_{3/2}$, the $6P_{3/2} \rightarrow 7D_{5/2}$, or the $6P_{1/2} \rightarrow 8S_{1/2}$ transition and the absorption of the probe intensity was monitored using photomultiplier PMT4 (Hamamatsu R928). In this case, the probe beam was chopped, but the pump beam was not (see Fig. 2).

The transmission of the probe-laser beam through a length L of the vapor is given by

$$I_\omega(L) = I_\omega(0) e^{-k_{n'l', j' \leftarrow 6P_J}(\omega)L} = I_\omega(0) e^{-\sigma_{n'l', j' \leftarrow 6P_J}(\omega) n_{6P_J} L} \quad (18)$$

for light of frequency ω . Here $I_\omega(0)$ is the incident intensity, $\sigma_{n'l', j' \leftarrow 6P_J}$ is the absorption cross section at frequency ω , and n_{6P_J} is the density of atoms in the lower state of the probe transition (which is assumed to be independent of z). Equation (18) can be solved for n_{6P_J} as

$$n_{6P_J} = \frac{1}{\sigma_{n'l', j' \leftarrow 6P_J} L} \ln \left(\frac{I_\omega(0)}{I_\omega(L)} \right). \quad (19)$$

We carried out calculations of the maximum absorption cross sections of each of the three probe transitions used in the experiment, based on oscillator strengths given by Warner [38], and hyperfine level branching ratios calculated from the formulas of Condon and Shortley [41]. Hyperfine level splittings were taken from Ref. [42] and each component was modeled as a Voigt line with Lorentzian width determined by resonance broadening in the lower level, and Gaussian width determined by Doppler broadening at the particular cell temperature. The absorption cross section was calculated as a function of frequency, and the maximum of this function was used with the measured maximum probe-laser beam attenuation in Eq. (19) to obtain an absolute determination of the excited-atom density. The spatial distribu-

tion of excited atoms was mapped from the measured probe-beam absorption versus position as the probe beam was translated across the cell diameter parallel to the pump beam.

IV. RESULTS AND DISCUSSION

Position dependent $6P_J$ state densities, $n_{6P_J}(x)$, were recorded as described in Sec. III. These values, and their squares were numerically integrated over the observation zone (cell diameter) to yield the factors $\int_{-R}^R n_{6P_J}(x) dx / \int_{-R}^R [n_{6P_J}(x)]^2 dx$ in Eq. (7). The $6P_J$ densities were also used in Eqs. (8)–(11), with the hyperfine level splittings of Ref. [42] and the resonance broadening rates of Ref. [43], to calculate the transmission factors $T_{6P_J \rightarrow 6S_{1/2}}$. Measured values of $[n_{6P_J}(r)]^2$ were used to calculate the radiation diffusion mode amplitudes a_j [Eq. (13)] for the $7P_{J'} \rightarrow 6S_{1/2}$ transitions. These amplitudes, in turn, were combined with the oscillator strengths of Warner [38] to find the effective radiative rates $\Gamma_{7P_{J'} \rightarrow 6S_{1/2}}^{\text{eff}}$ using Eqs. (14)–(16). Effective radiative rates for the fundamental radiation diffusion mode were determined using the measured $6P_J$ atom density and spatial distribution for relevant transitions, as described in Sec. II B. Finally, the effective and natural radiative rates were summed to obtain the effective lifetimes $\tau_{nl_{J'}}^{\text{eff}}$ as in Eq. (12). All of this information was then combined with the measured fluorescence ratios (corrected for detection system efficiency) in Eq. (7) to yield values for the various energy-pooling rate coefficients. The rate coefficient values obtained for different transitions and at different temperatures are given in Table I.

Despite the care that was taken in accounting for the $6P_J$ spatial distribution and radiation trapping on all transitions of interest, it is clear from Table I that significant discrepancies exist between values of $k_{7P_{J'}}$, or values of $k_{6D_{3/2}}$, taken at different temperatures or with different pump geometries. This is, in part, due to the fact that the uncertainties in individual measurements are fairly large. Fluorescence ratios probably have an uncertainty of as much as 25% due to the use of neutral density filters to attenuate the D_1 and D_2 line fluorescence. We estimate the uncertainties in the ratio $\int_{-R}^R n_{6P_J}(x) dx / \int_{-R}^R [n_{6P_J}(x)]^2 dx$ to be approximately 15%. Uncertainties in $T_{nl_{J'} \rightarrow n'l'_{J''}}$ and $\tau_{nl_{J'}}^{\text{eff}}$ largely offset each other when the product $T_{nl_{J'} \rightarrow n'l'_{J''}} (\tau_{nl_{J'}}^{\text{eff}} / \tau_{nl_{J'}}^{\text{nat}})$ is taken. This is because an over estimation of the amount of radiation trapping results in a transmission factor which is too low, but an effective lifetime which is too high. Values of $T_{7P_{3/2} \rightarrow 6S_{1/2}} (\tau_{7P_{3/2}}^{\text{eff}} / \tau_{7P_{3/2}}^{\text{nat}})$ are probably good to within 25%, while the values of $T_{7P_{1/2} \rightarrow 6S_{1/2}} (\tau_{7P_{1/2}}^{\text{eff}} / \tau_{7P_{1/2}}^{\text{nat}})$ are accurate to at least 10% because the trapping is much less severe on this transition. Similarly, even though the $6P_J$ densities are non-uniform, which considerably complicates the calculation of trapping corrections for transitions which terminate on these levels, the values of $T_{nl_{J'} \rightarrow n'l'_{J''}} (\tau_{nl_{J'}}^{\text{eff}} / \tau_{nl_{J'}}^{\text{nat}})$ for the $4F$, $8S$, and $6D$ states are accurate to within 15% (except in one or two cases) since both corrections are small and tend to cancel. Finally, the largest source of statistical uncertainty in the rate coefficients listed in Table I is that due to $T_{6P_J \rightarrow 6S_{1/2}}$. These transmission factors are as small as 0.004 and they

may be uncertain by as much as 30–40%, due primarily to the assumption that the ground-state hyperfine level populations are in a statistical ratio. Considering these various sources of statistical uncertainty, we estimate overall errors of $\sim 50\%$ in our measured energy-pooling rate coefficients.

In addition, various other systematic effects and uncertainties should also be considered before we arrive at final energy-pooling rate coefficients. First, the cesium ground-state atom density was obtained from the Nesmeyanov vapor pressure formula [39] and the measured temperature. We estimate the uncertainty in the ground-state density at 5–10% in our temperature range, but this uncertainty only affects the energy-pooling results through its influence on the transmission factors and $7P_{J'}$ effective lifetimes, where it is roughly a linear effect in the Doppler broadened limit [29,30]. Second, all oscillator strengths used in this work were taken from the theoretical paper of Warner [38], since a complete and self-consistent set is available in this one reference. However, considerable discrepancy exists between various sets of theoretical oscillator strengths for cesium [38,44–47], and any systematic errors in the chosen values will directly introduce systematic errors in our final results. Based on the various available oscillator strengths, we estimate uncertainties in $\Gamma_{nl_{J'} \rightarrow n'l'_{J''}}^{\text{nat}}$ ranging from 2% to 23% for the $6D \rightarrow 6P$ and $8S \rightarrow 6P$ transitions. However, for $7P_{J'} \rightarrow 6S_{1/2}$ the uncertainty can be more than a factor of 2. Thus, the $4F_{5/2,7/2}$, $8S_{1/2}$ and $6D_{3/2,5/2}$ energy-pooling rates are not seriously affected by uncertainty in the oscillator strengths, but the $7P_{J'}$ rates can be strongly affected.

As can be seen from the rate equation for the state $nl_{J'}$ [Eq. (2)], we have neglected cascade from higher-lying levels which are also populated by the energy-pooling process. Inclusion of this process would involve the addition of a term $\sum_{n''l''_{J''}} \Gamma_{n''l''_{J''} \rightarrow nl_{J'}}^{\text{eff}} n_{n''l''_{J''}}$ to the right-hand side of Eq. (2). From the radiative rates of Warner (modified by trapping calculations where needed) and the measured energy-pooling rate coefficients (Table I) we find that cascade processes do not affect our D_1 pumping results by more than 10% in the worst case. For D_2 pumping, we find that both $6D$ and $8S$ cascade could be responsible for major contributions to the $7P$ signals. However the error bars on k_{8S} are quite large and the rate coefficient may be strongly temperature dependent since energy pooling to $8S$ is highly endothermic ($8S$ fluorescence signals were small and very noisy at temperatures below 85 °C). Moreover, if the $7P$ signals in the D_2 pumping case are due primarily to $8S \rightarrow 7P$ cascade, we would expect to see $7P_{3/2} \rightarrow 6S_{1/2}$ fluorescence signals that are twice as large as the $7P_{1/2} \rightarrow 6S_{1/2}$ signals, and experimentally this is not the case. Thus we can neither confirm nor rule out a significant cascade contribution to the $7P$ signals in the D_2 pumping case.

We must also consider collisional mixing among fine-structure levels (i.e., $7P_{3/2} + M \leftrightarrow 7P_{1/2} + M$) and collisional excitation transfer processes such as $6D + M \leftrightarrow 7P + M$, where M is a ground-state cesium or impurity atom. Such processes can also distort the apparent energy-pooling rate coefficients. We can estimate the concentration of impurities in our sealed cell by analysis of the ratio of sensitized fluorescence (i.e., fluorescence from the level $6P_{J'}$ that is not pumped by the laser) to direct fluorescence at room tempera-

ture. The measured ratio is much too large to be explained by cesium-cesium collisions according to the experimental cross sections of Czajkowski and Krause [48], and thus must be attributed to collisions with impurities. Czajkowski, McGillis, and Krause [49] have investigated excitation transfer among the cesium $6P_J$ levels due to collisions with inert gas atoms, but their measured cross sections, which range from 2×10^{-21} to 3×10^{-19} cm², are also much too small to account for the amount of transfer we observe in our sealed cell. However, the impurities in our cell are more likely to be diatomic molecules which possess internal degrees of freedom, and excitation transfer in collisions of cesium $6P_J$ atoms with such molecules is likely to involve relatively large rate coefficients. If we assume an excitation transfer rate coefficient of 10^{-10} cm³ s⁻¹, then an impurity gas pressure of $\sim 3.7 \times 10^{-3}$ Torr ($\sim 1 \times 10^{14}$ cm⁻³ impurity density) is required to produce the observed population transfer. Based upon this impurity density, and assuming relatively large rate coefficients for various excitation transfer processes (see, e.g., Refs. [50–54]), we can show that $8S \leftrightarrow 4F$ transfer by impurities contributes less than 10% uncertainty to our energy-pooling rates in the worst case, and that $6D \rightarrow 7P$ collisional excitation transfer produces an effect on the energy-pooling results which is comparable to that of $6D \rightarrow 7P$ radiative cascade. Excitation transfer within the $7P_{J'}$ and $6D_{J'}$ manifolds, due to collisions with impurities or ground-state cesium atoms, can cause a skewing of the ratio of the energy-pooling rates to the various fine-structure levels. This is probably the cause of the decrease of $k_{7P_{1/2}}/k_{7P_{3/2}}$ with increasing temperature for both D_1 and D_2 line pumping.

Finally, we note that in this experiment we only measure the population of atoms in the directly excited $6P_J$ fine-structure level. However, due to excitation transfer from one fine-structure level to the other (induced by collisions with ground-state atoms and impurities) there is always some population in the other $6P_J$ level as well. The density in the collisionally populated level is too small to be measured using our absorption technique, but it can be inferred from the D_1/D_2 line fluorescence ratio. At the highest temperature used in this experiment, we find that the density ratio of atoms in the collisionally populated level to those in the level directly populated by the laser is less than 0.04. From the rate coefficients given in Table I and the relative populations, it is clear that $6P_{1/2}$ - $6P_{1/2}$ collisions cannot significantly influence the results obtained for the $6P_{3/2}$ - $6P_{3/2}$ rates and vice versa. However, $6P_{1/2}$ - $6P_{3/2}$ collisions might have a systematic effect on these results, since the rate coefficients for the latter process could be significantly greater than those for $6P_{3/2}$ - $6P_{3/2}$, where the energy defect for $nl=7P$ or $6D$ in Eq. (1) is considerably smaller for $1/2$ - $3/2$ collisions than for $3/2$ - $3/2$ collisions. For the $6D$ product state, the $1/2$ - $3/2$ energy deficit is comparable to the $1/2$ - $1/2$ deficit, but it is positive for $1/2$ - $3/2$ collisions and negative for $1/2$ - $1/2$ collisions. Similarly, $1/2$ - $3/2$ collisions may significantly affect the measured $1/2$ - $1/2$ rate coefficient for populating $8S$. At present, we have no way to estimate the magnitude of this effect (which we plan to investigate through a two-laser excitation experiment). It is possible that this effect is responsible for the slight increase in the apparent energy-pooling rate coefficients $k_{7P_{1/2}}$ and $k_{7P_{3/2}}$ with increasing temperature

when pumping the D_2 transition.

Considering only the statistical sources of uncertainties, we have determined a set of best values of the measured rate coefficients which is presented in Table II. However, it should be kept in mind that the overall accuracy of these results may be limited by the various systematic effects discussed above.

V. CONCLUSIONS

The energy-pooling rate coefficients reported here can be expressed as velocity-averaged cross sections using the relation

$$k_{nlJ'} = \langle \sigma_{nlJ'}(v)v \rangle \approx \sigma_{nlJ'} \bar{v}. \quad (20)$$

Here $\sigma_{nlJ'}(v)$ and $\sigma_{nlJ'}$ are the velocity-dependent and velocity-averaged cross sections, respectively, v is the collision velocity, and \bar{v} is the mean collision velocity given by

$$\bar{v} = \left(\frac{8RT}{\pi} \frac{M_1 + M_2}{M_1 M_2} \right)^{1/2} = 1.78 \times 10^3 T^{1/2} \text{ cm/s}. \quad (21)$$

In this last expression, $R=8.31$ J/(K mole) is the gas constant, T is the absolute temperature, and M_1 and M_2 are the molar masses of the two colliding atoms. The last equality in Eq. (21) is appropriate for collisions between two cesium atoms ($M_1 = M_2 = 0.1329$ kg/mole).

Values of σ_{nl} for the energy-pooling processes studied in this work (obtained by averaging all data collected over the range 337–365 K) are presented in Table II along with the few values that have been obtained by other authors. Our cross sections for energy pooling to the $6D$ levels are consistent with the experimental estimates of Klyucharev and Lazarenko [1] and Yabuzaki *et al.* [18] as well as with the theoretical estimate of Borodin and Komarov [17]. Our values of the rate coefficients for the process $\text{Cs}(6P_{3/2}) + \text{Cs}(6P_{3/2}) \rightarrow \text{Cs}(7P_{1/2,3/2}) + \text{Cs}(6S_{1/2})$ obtained at low density are in agreement within the rather large error bars with the values we have obtained under very different experimental conditions [19,20].

The results of Table II show that $6P_{1/2} + 6P_{1/2}$ collisions are more effective than $6P_{3/2} + 6P_{3/2}$ collisions at populating the $7P_{J'}$ levels. This is expected from consideration of the energy deficits. Similarly, $8S$ and $4F$ are populated much more effectively by $3/2$ - $3/2$ than by $1/2$ - $1/2$ collisions. In addition, when pumping with D_1 light, $7P_{1/2}$ is two to three times more likely to be populated than $7P_{3/2}$. For D_2 pumping, $7P_{1/2}$ and $7P_{3/2}$ are approximately equally populated. For the $6D_{J'}$ levels we find that $6D_{3/2}$ is more strongly populated than $6D_{5/2}$ by $1/2$ - $1/2$ collisions while $6D_{5/2}$ is more strongly populated than $6D_{3/2}$ by $3/2$ - $3/2$ collisions. However, in the latter case, the error bars are large and not much data exists. Thus these conclusions must be taken with a grain of salt. In previous studies of energy pooling in Sr [10,55] and Ba [15] it was found that the energy deficit does not play a strong role in determining the rate coefficients. In Sr, the rates fall off somewhat with ΔE for endothermic processes, since only a fraction of collision pairs have a relative kinetic energy greater than ΔE . In the case of Ba, the energy-pooling rates are largely independent of energy defi-

TABLE II. Best values for the cesium energy-pooling rate coefficients and cross sections obtained in this work, along with those obtained by other workers.

$\text{Cs}(6P_{3/2}) + \text{Cs}(6P_{3/2}) \rightarrow \text{Cs}(nl_{J'}) + \text{Cs}(6S_{1/2})$				
$nl_{J'}$	Rate coefficient ($\text{cm}^3 \text{s}^{-1}$)		Cross section (cm^2)	
	This work (a)	Other values	This work (a)	Other values
$7P_{1/2}$	$(5.9 \pm 2.7) \times 10^{-12}$	$(3.1 \pm 1.6) \times 10^{-12}$ (b)	$(1.8 \pm 0.8) \times 10^{-16}$	$(0.9 \pm 0.5) \times 10^{-16}$ (b)
$7P_{3/2}$	$(6.1 \pm 3.1) \times 10^{-12}$	$(3.8 \pm 1.9) \times 10^{-12}$ (b)	$(1.8 \pm 0.9) \times 10^{-16}$	$(1.1 \pm 0.5) \times 10^{-16}$ (b)
$6D_{3/2}$	$(9.0 \pm 2.9) \times 10^{-11}$	$< 4 \times 10^{-9}$ (c) $> 6 \times 10^{-11}$ (d)	$(2.7 \pm 0.9) \times 10^{-15}$	$< 10^{-13}$ (c) $> 1.5 \times 10^{-15}$ (d)
$6D_{5/2}$	$(1.9 \pm 1.0) \times 10^{-10}$	$(6.2^{+6.2}_{-2.9}) \times 10^{-10}$ (e) $< 4 \times 10^{-9}$ (c) $> 6 \times 10^{-11}$ (d)	$(5.6 \pm 2.8) \times 10^{-15}$	$(1.5^{+1.5}_{-0.7}) \times 10^{-14}$ (e) $< 10^{-13}$ (c) $> 1.5 \times 10^{-15}$ (d)
$4F_{5/2}$	$(1.2 \pm 0.6) \times 10^{-11}$		$(3.6 \pm 1.8) \times 10^{-16}$	
$4F_{7/2}$	$(2.0 \pm 1.0) \times 10^{-11}$		$(6.0 \pm 3.0) \times 10^{-16}$	
$8S_{1/2}$	$(1.7 \pm 0.8) \times 10^{-11}$		$(5.2 \pm 2.2) \times 10^{-16}$	
$\text{Cs}(6P_{1/2}) + \text{Cs}(6P_{1/2}) \rightarrow \text{Cs}(nl_{J'}) + \text{Cs}(6S_{1/2})$				
$nl_{J'}$	Rate coefficient ($\text{cm}^3 \text{s}^{-1}$)		Cross section (cm^2)	
	This work (a)	Other values	This work (a)	Other values
$7P_{1/2}$	$(1.3 \pm 0.6) \times 10^{-10}$		$(3.8 \pm 1.8) \times 10^{-15}$	
$7P_{3/2}$	$(4.5 \pm 1.4) \times 10^{-11}$		$(1.3 \pm 0.4) \times 10^{-15}$	
$6D_{3/2}$	$(4.4 \pm 0.9) \times 10^{-10}$	$< 4 \times 10^{-9}$ (c) $> 6 \times 10^{-11}$ (d)	$(1.3 \pm 0.3) \times 10^{-14}$	$< 10^{-13}$ (c) $> 1.5 \times 10^{-15}$ (d)
$6D_{5/2}$	$(2.7 \pm 1.4) \times 10^{-10}$	$(6.2^{+6.2}_{-2.9}) \times 10^{-10}$ (e) $< 4 \times 10^{-9}$ (c) $> 6 \times 10^{-11}$ (d)	$(8.0 \pm 4.0) \times 10^{-15}$	$(1.5^{+1.5}_{-0.7}) \times 10^{-14}$ (e) $< 10^{-13}$ (c) $> 1.5 \times 10^{-15}$ (d)
$4F_{5/2}$	$< 3 \times 10^{-11}$		$< 8 \times 10^{-16}$	
$4F_{7/2}$	$< 3 \times 10^{-11}$		$< 8 \times 10^{-16}$	
$8S_{1/2}$	$(1.1 \pm 0.6) \times 10^{-12}$		$(3.3 \pm 1.7) \times 10^{-17}$	

^a $T = 337 - 365$ K. Note that error bars given in the table reflect statistical uncertainties only. We believe that these values are probably accurate to within $\sim 50\%$ when estimates of possible systematic uncertainties are included. See text.

^bExperimental values from Ref. [19]. $T = 370$ K.

^cUpper limit from experimental work of Ref. [1]. $T = 528$ K.

^dLower limit from theoretical work of Ref. [17]. $T = 500$ K.

^eExperimental estimate of rate coefficient for the inverse process $\text{Cs}(6D_{3/2}) + \text{Cs}(6S_{1/2}) \rightarrow \text{Cs}(6P) + \text{Cs}(6P)$. $T = 530$ K. From Ref. [18].

cit, even for endothermic processes. This surprising result was attributed, in part, to the fact that levels with the largest energy deficit also have the largest statistical weights [15]. In addition, these studies found no strong angular-momentum propensity rules. High-lying singlet and triplet states were populated with approximately equal rates, and although levels with higher L values are more strongly populated than those with lower L values, this may also be due to the higher statistical weights of the former [15]. These effects were ascribed to the breakdown of LS coupling in the heavy Sr and Ba atoms. Because of this breakdown, propensity rules concerning total electronic angular momentum J might be more relevant. The Sr and Ba results indicate that 1F_3 states are strongly populated by $^1P_1 + ^1P_1$ and $^3P_1 + ^3P_1$ collisions. Our present results for cesium indicate a contrary trend. Here we also find a breakdown of LS coupling in cesium, which lies next to barium in the periodic table. However, in cesium all relevant levels are spin doublets, and thus spin changing collisions are not observable in the present experiment. Nevertheless, the fairly dramatic difference between the ratio of $7P_{1/2}$ and $7P_{3/2}$ energy-pooling rate coefficients for D_1 vs

D_2 pumping seems to indicate that, in some cases, angular momentum may play a role in the energy-pooling process, such that processes which require the conversion of angular momentum associated with the orbital motion of the two colliding atoms, into internal electronic angular momentum, occur with lower rates.

In the near future, we plan to extend the present set of measurements by adding another laser to the experimental setup. With this modification, we will be able to simultaneously populate the $6P_{1/2}$ and $6P_{3/2}$ levels, and thus we will be able to study the $6P_{1/2} + 6P_{3/2}$ collisions which may have the largest energy-pooling cross sections.

ACKNOWLEDGMENTS

Financial support for this work was provided by the National Science Foundation under Grant PHY-9119498. The authors from Pisa also acknowledge support from the EEC Network Grant ERBCHRXCT 930344. One of the authors (S.M.) is grateful to ICTP, Trieste, for financial support during his stay in Pisa.

- [1] A. N. Klyucharev and A. V. Lazarenko, *Opt. Spectrosc.* **32**, 576 (1972); [*Opt. Spektrosk.* **32**, 1063 (1972)].
- [2] For a review of alkali-metal atom energy-pooling cross-section measurements until 1985, see M. Allegrini, C. Gabbanini, and L. Moi, *J. Phys. Colloq. C1* **46**, C1-61 (1985).
- [3] M. Allegrini, C. Gabbanini, L. Moi, and R. Colle, *Phys. Rev. A* **32**, 2068 (1985).
- [4] S. A. Davidson, J. F. Kelly, and A. Gallagher, *Phys. Rev. A* **33**, 3756 (1986).
- [5] C. He and R. A. Bernheim, *Chem. Phys. Lett.* **190**, 494 (1992).
- [6] S. Gozzini, S. A. Abdullah, M. Allegrini, A. Cremoncini, and L. Moi, *Opt. Commun.* **63**, 97 (1987).
- [7] C. Gabbanini, S. Gozzini, G. Squadrito, M. Allegrini, and L. Moi, *Phys. Rev. A* **39**, 6148 (1989).
- [8] W. H. Breckenridge, W. L. Nikolai, and J. Stewart, *J. Chem. Phys.* **74**, 2073 (1981).
- [9] H. Umemoto, J. Kikuma, A. Masaki, and S. Sato, *Chem. Phys.* **127**, 227 (1988).
- [10] J. F. Kelly, M. Harris, and A. Gallagher, *Phys. Rev. A* **38**, 1225 (1988).
- [11] S. Majetich, C. A. Tomczyk, and J. R. Wiesenfeld, *Phys. Rev. A* **41**, 6085 (1990).
- [12] H. G. C. Werij, M. Harris, J. Cooper, A. Gallagher, and J. F. Kelly, *Phys. Rev. A* **43**, 2237 (1991).
- [13] B. Cheng, Z. Li, Y. Yang, J. Zhu, and D. Zhang, *Opt. Commun.* **86**, 465 (1991).
- [14] P. Bicchi, C. Marinelli, E. Mariotti, M. Meucci, and L. Moi, *J. Phys. B* **26**, 2335 (1993).
- [15] J. A. Neuman, A. Gallagher, and J. Cooper, *Phys. Rev. A* **50**, 1292 (1994).
- [16] For a review, see T. Walker and P. Feng, in *Advances in Atomic, Molecular and Optical Physics*, edited by B. Bederson and H. Walther (Academic, San Diego, 1994), Vol. 34, p. 125.
- [17] V. M. Borodin and I. V. Komarov, *Opt. Spectrosc.* **36**, 145 (1974); [*Opt. Spektrosk.* **36**, 250 (1974)].
- [18] T. Yabuzaki, A. C. Tam, M. Hou, W. Happer, and S. M. Curry, *Opt. Commun.* **24**, 305 (1978).
- [19] S. Milošević, F. de Tomasi, F. Fuso, and M. Allegrini, *Europhys. Lett.* **32**, 703 (1995).
- [20] F. de Tomasi, S. Milošević, P. Verkerk, A. Fioretti, M. Allegrini, Z. J. Jabbour, and J. Huennekens (unpublished).
- [21] N. N. Bezuglov, A. N. Klucharev, and V. A. Sheverev, *J. Phys. B* **20**, 2497 (1987).
- [22] W. Gautschi, *SIAM (Soc. Ind. Appl. Math.) J. Numer. Anal.* **7**, 187 (1970).
- [23] W. Gautschi, *Commun. ACM* **12**, 635 (1969).
- [24] D. G. Hummer, *Mem. R. Astronom. Soc.* **70**, 1 (1965).
- [25] B. P. Kibble, G. Copley, and L. Krause, *Phys. Rev.* **153**, 9 (1967).
- [26] J. Huennekens and A. Gallagher, *Phys. Rev. A* **28**, 238 (1983).
- [27] A. Romberg and H.-J. Kunze, *J. Quant. Spectrosc. Radiat. Transfer* **39**, 99 (1988).
- [28] T. Colbert and J. Huennekens, *Phys. Rev. A* **41**, 6145 (1990).
- [29] T. Holstein, *Phys. Rev.* **72**, 1212 (1947).
- [30] T. Holstein, *Phys. Rev.* **83**, 1159 (1951).
- [31] E. A. Milne, *J. London Math. Soc.* **1**, 40 (1926).
- [32] A. F. Molisch, B. P. Oehry, and G. Magerl, *J. Quant. Spectrosc. Radiat. Transfer* **48**, 377 (1992).
- [33] A. F. Molisch, B. P. Oehry, W. Schupita, and G. Magerl, *J. Quant. Spectrosc. Radiat. Transfer* **49**, 361 (1993).
- [34] J. Huennekens, R. K. Namiotka, J. Sagle, Z. J. Jabbour, and M. Allegrini, *Phys. Rev. A* **51**, 4472 (1995).
- [35] M. G. Payne and J. D. Cook, *Phys. Rev. A* **2**, 1238 (1970).
- [36] C. van Trigt, *Phys. Rev. A* **13**, 726 (1976).
- [37] J. Huennekens and T. Colbert, *J. Quant. Spectrosc. Radiat. Transfer* **41**, 439 (1989).
- [38] B. Warner, *Mon. Not. R. Astron. Soc.* **139**, 115 (1968).
- [39] A. N. Nesmeyanov, *Vapour Pressure of the Elements* (Academic, New York, 1963).
- [40] R. Stair, W. E. Schneider, and J. K. Jackson, *Appl. Opt.* **2**, 1151 (1963).
- [41] E. U. Condon and G. H. Shortley, *The Theory of Atomic Spectra* (Cambridge University Press, New York, 1977), pp. 63–69. See also M. Arditì, I. Hirano, and P. Tougne, *J. Phys. D* **11**, 2465 (1978).
- [42] E. Arimondo, M. Inguscio, and P. Violino, *Rev. Mod. Phys.* **49**, 31 (1977).
- [43] Z. J. Jabbour, J. Sagle, R. K. Namiotka, and J. Huennekens, *J. Quant. Spectrosc. Radiat. Transfer* **54**, 767 (1995).
- [44] O. S. Heavens, *J. Opt. Soc. Am.* **51**, 1058 (1961).
- [45] P. M. Stone, *Phys. Rev.* **127**, 1151 (1962).
- [46] M. Fabry and J. R. Cussenot, *Can. J. Phys.* **54**, 836 (1976).
- [47] S. S. Liaw, *Can. J. Phys.* **70**, 1279 (1992).
- [48] M. Czajkowski and L. Krause, *Can. J. Phys.* **43**, 1259 (1965).
- [49] M. Czajkowski, D. A. McGillis, and L. Krause, *Can. J. Phys.* **44**, 91 (1966).
- [50] J. Berlande, quoted in the article by L. Krause, in *The Excited State in Chemical Physics*, edited by J. W. McGowan (Wiley, New York, 1975), pp. 267–316.
- [51] J. Cuvellier, P. R. Fournier, F. Gounand, J. Pascale, and J. Berlande, *Phys. Rev. A* **11**, 846 (1975).
- [52] A. C. Tam, T. Yabuzaki, S. M. Curry, M. Hou, and W. Happer, *Phys. Rev. A* **17**, 1862 (1978).
- [53] I. N. Siara, R. U. Dubois, and L. Krause, *Can. J. Phys.* **60**, 239 (1982).
- [54] J. Supronowicz, J. B. Atkinson, and L. Krause, *Phys. Rev. A* **31**, 2691 (1985).
- [55] H. G. C. Werij, M. Harris, J. Cooper, and A. Gallagher, *Phys. Rev. A* **43**, 2237 (1991).
- [56] C. E. Moore, *Atomic Energy Levels*, Natl. Bur. Stand. (U.S.) Circ. No. 467 (U.S. GPO, Washington, D.C., 1948, 1952, and 1958), Vols. I-III.